Effect of environmental media on ablation rate of stainless steel under femtosecond laser multiple raster scans

Zeqin Cui (崔泽琴)[1,2*], Yingqi Li (黎颖奇)[1], Wenxian Wang (王文先)[1,2], Chenghsiang Lin (林振祥)[3], and Bingshe Xu (许并社)[2]

[1]College of Material Science and Engineering, Taiyuan University of Technology, Taiyuan 030024, China

[2]Key laboratory of Interface Science and Engineering in Advanced Materials of Ministry of Education, Taiyuan 0300 24, China

[3]Department of Mechanical and Aerospace Engineering, Missouri University of Science and Technology, Rolla, MO 65409, USA

[*]Corresponding author: cuizeqin@tyut.edu.cn

Received September 17, 2014; accepted November 28, 2014; posted online January 4, 2015

We investigate the influence of environmental media on ablation rate of AISI 443 stainless steel under femtosecond (fs) laser single raster scan and multiple raster scans in air, water, and methanol. Meanwhile, the development of ablation rate with the change of fs laser-induced surface morphology in the three environmental media is comparatively studied. The results show that environmental media as well as fs laser-induced morphology control the ablation rate with the increasing number of raster scans (N). Under single raster scanning ($N = 1$), the ablation rate is higher in liquid than in air due to the confinement of plasma, laser-induced shockwaves, and bubble-related mechanical forces. However, under multiple raster scans, the variation in ablation rate with the increase in N in these three environmental media is complicated and is largely determined by the surface morphology induced by previous fs laser ablation. When $N > 20$, the ablation rate is much higher in air than in liquids due to preferential ablation caused by the formation of nanostructures-textured mound-shaped microstructures in air. Besides, the redeposition of ejected ablated materials is also an important factor that affects the ablation depth.

OCIS codes: 140.7090, 320.2250, 350.3850, 240.6700.

doi: 10.3788/COL201513.011402.

Surface morphology can significantly influence surface properties of solid materials, such as optical, wetting, chemical, biological, and other properties[1]. It has been demonstrated that femtosecond (fs) laser-induced surface micro/nanostructures can modify optical or wetting properties of solids, for example, enhancing optical absorption[2,3], creating structural colors[4], and producing superhydrophobic surface[5]. Thus, fs laser surface micro/nanostructuring has important application potential in laser damage[6], solar absorbers[7], identifying codes[8], photonics[9], nano/microfluidics, optofluidics, biomedicine, and so on[1].

A large variety of fs laser-induced surface micro/nanostructures have been studied on various materials, such as fs laser-induced periodic surface structures or ripples[10–15], irregular nanostructures[16,17], and nanostructures-textured microstructures[18–21]. Many studies have focused on discussing the influence of environmental media[21–26] or laser parameters on the formation of fs laser-induced surface micro/nanostructures, or on the optical or wetting properties of solids. Besides, almost all of these studies were conducted under fs laser stationary multi-pulse irradiation or single raster scan.

Fs laser surface micro/nanostructuring is based on fs laser ablation. The ablation depth of fs laser is of the order of 0.01–1 μm per pulse. Hence, fs laser ablation can be very precise. However, at the same time, fs laser ablation is low throughput due to low ablation efficiency, which is not suitable for industrial applications[27]. The ablation medium (air, gas, or liquid) has significant influence on ablation rate. Previous studies have proved that the presence of liquid can enhance ablation efficiency[28–30]. Besides, Jiao *et al.*[30] found that compared with water, more volatile liquids, such as methanol, are more effective in increasing ablation rate and reducing debris formation during the fs laser drilling process.

In this letter, we comparatively study fs laser ablation of 443 stainless steel (SS) in air, water, and methanol media under multiple raster scans. The formation mechanisms of surface micro/nanostructures formed in these three environmental media will be discussed in our subsequent work. In this letter, we focus on studying the effect of environmental media on the ablation rate under fs laser multiple raster scans. Compared with single raster scan, under multiple raster scans, the surface morphology produced by previous ablations will significantly affect the absorbed laser intensity of subsequent ablation and then affect the ablation rate. We show that the variation of ablation depth becomes

more complicated during fs laser multiple raster scans in different environmental media due to different properties of environmental media and continuous change of surface morphology. Despite intensive studies, the formation mechanisms of fs laser-induced surface micro/nanostructures are not yet fully understood. The discussion on ablation rate in different environmental media under fs laser multiple raster scans will be highly useful to further understand the interaction between fs laser and materials.

AISI 443 ferritic SS with a thickness of 1 mm was used in this experiment. Before laser irradiation, each sample surface was kept in its initial state without mechanical polishing. The surface roughness (R_a) of SS was about 0.049 μm. An amplified Ti:Sapphire fslaser (Legend-F, Coherent) delivered horizontally polarized laser with the pulse duration of 120 fs, the central wavelength of 800 nm and the repetition rate of 1 kHz were employed to ablate SS samples. The laser beam was focused by a lens with 100 mm focal length and was perpendicular to the sample surface. The radius of the spot (defined at $1/e^2$ of the beam intensity) was about 12 μm.

The samples were mounted on a computer controlled five-axis motion stage with a resolution of 1 μm, and an in-line imaging system was used to real-time monitor the ablation process. The laser beam and each sample's position in the Z-direction were fixed. Each sample was horizontally translated line by line with a step size of 14 μm between lines to ablate the surface over an area of 1×0.2 (mm). In the process of multiple raster scans, the samples were repeatedly irradiated in the same places with different numbers of raster scans. The number of raster scans (N) ranged from 1 to 400. The scanning rate (v) and the laser fluence (F) were 2 mm/s and 1.327 J/cm^2, respectively.

The SS samples were irradiated in air, water, and methanol, respectively. Table 1 summarizes the physicochemical properties of methanol and water used as assist liquids. Methanol has lower boiling point, surface tension, and enthalpy of vaporization (EVP) as compared with water. When using liquids as environmental media, the specimens were immersed in the liquid with about 5 mm of liquid thickness above the surface.

Before and after ablation, the samples were cleaned in an ultrasonic bath in acetone and then in ethanol each for 10 min. A field emission scanning electron microscope (SEM; JSM-7001F, JEOL) and an ultraviolet laser scanning confocal microscope (LSCM; LEXT OLS4100, Olympus) were used to examine the surface morphology of the samples after fs laser irradiation.

Table 1. Physicochemical Properties of Liquids Used in Laser Ablation

Physicochemical Property	Water	Methanol
Molecular Formula	H_2O	CH_3OH
Surface Tension (mN/m)	71.9	22.6
Density (g/cm^3)	1.00	0.79
Boiling Point (°C)	100	64.7
EVP (kJ/mol)	40.65	35.3

A series of SEM images showing the development of surface morphology with the increase in N in air, water, and methanol are shown in Fig. 1. The black arrow with E indicates the laser polarization direction which is parallel to the laser scanning direction. Figures 2–4 are LSCM height images of fs laser ablated sample surfaces in air, water, and methanol, respectively. The black arrow in Figs. 2–4(a) indicates the laser polarization direction which is parallel to the laser scanning direction. As shown in Figs. 1–4, in different environmental media, the surface morphologies changed significantly with the increase in N, which can be attributed to the differences in physicochemical properties between environmental media.

When irradiated in air, submicrometer-scale rough ripples oriented perpendicular to the laser polarization direction were induced when $N = 1$ (Fig. 1(a)). Increasing N to 5, precursor protrusions with base diameter less than 10 μm began to form on the ripples (Fig. 1(b)). When $N = 20$, some nanostructures-textured mound-shaped microstructures (N-mounds for short) were randomly produced on the ripples (Fig. 1(c)). Further increasing N to 100, linked N-mounds were formed over

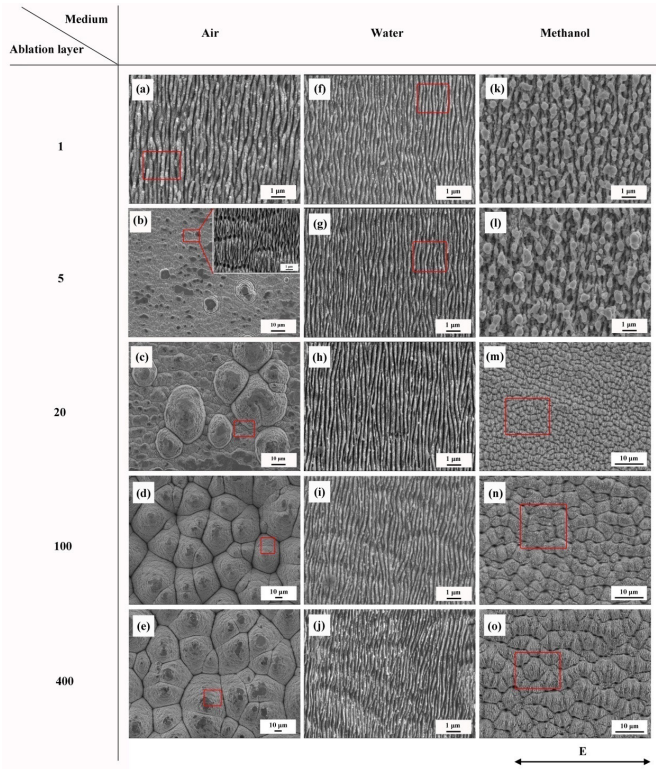

Fig. 1. A series of SEM images showing the development of surface morphology with the increase in N: (a–e) in air, (f–j) in water, and (k–o) in methanol. The red borders express magnified area.

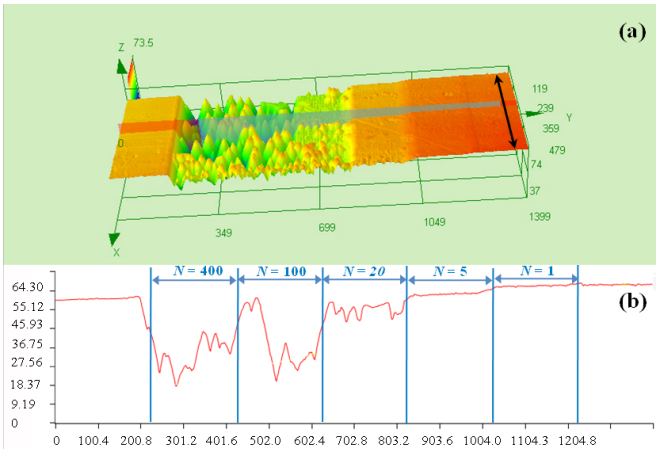

Fig. 2. LSCM height image of sample surface after fs laser irradiation in air: (a) overall 3D colorized image and (b) outline of the cross-section marked in (a).

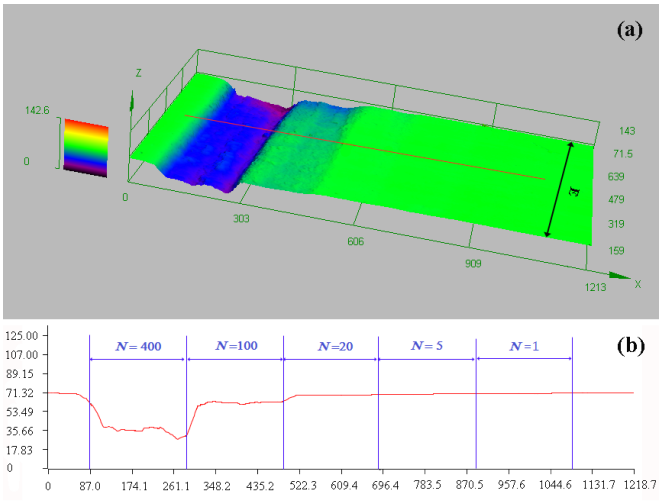

Fig. 3. LSCM height image of sample surface after fs laser irradiation in water: (a) overall 3D height image and (b) the outline of the cross-section marked in (a).

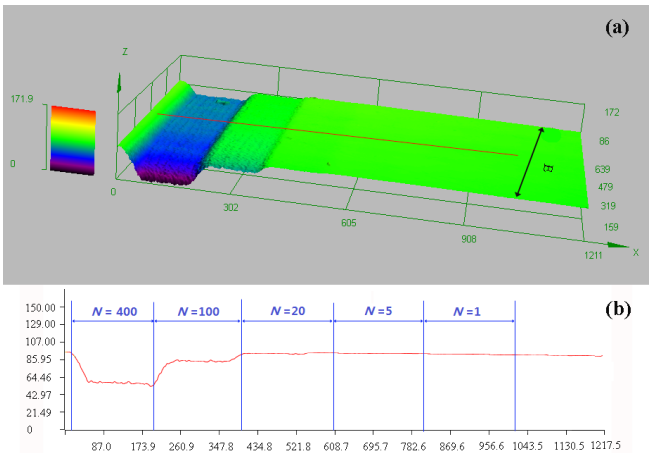

Fig. 4. LSCM height image of sample surface after fs laser irradiation in methanol: (a) overall 3D height image and (b) the outline of the cross-section marked in (a).

the entire irradiated area (Fig. 1(d)). However, once the linked N-mounds were fully formed, the surface morphology nearly did not change despite further increasing N to 400 (Fig. 1(e)).

When irradiated in water, the surface structures were all ripples perpendicular to the laser polarization direction with the increase in N (Figs. 1(f–j)). Compared with the ripples obtained in air, the ripples obtained in water were more smooth, straight, and compact. The ripples obtained when $N = 5$ and 20 were nearly parallel. The ripples tend to become discontinuous when $N = 100$ and some areas caved in when $N = 400$.

Even though methanol is also a liquid ablation medium, the surface structures experienced different transitions with the increase in N (Figs. 1(k–o)). Perpendicular ripples were also induced when $N = 1$ and 5. Both of them were uneven and rough ripples covered with submicrometer particles with diameters of 200—300 nm on the top of the surface. Increasing N to 20, horizontal grooves were formed on the perpendicular ripples, making the perpendicular ripples become discontinuous (Fig. 1(m)). With further etching of subsequent laser pulses, the grooves grew deeper and the segments constituting the perpendicular discontinuous ripples became longer (Fig. 1(n)). The adjacent ripple segments gathered together and had a tendency to form protrusions. Finally, ripples-textured microprotrusions were produced when $N = 400$ (Fig. 1(o)).

In order to know the variation of ablation depth with the increase in N in air, water, and methanol, we processed Figs. 2(b), 3(b), and 4(b). The ablation depth of each section is shown in Table 2 and Fig. 5. Note that the ablation depth presented in Table 2 is defined as the perpendicular distance from the untreated sample surface to the lowest point of each ablated section. Besides, the calculated ablation depth just presents a general variation tendency. It can be seen that the ablation depth increases with N in a nonlinear form. However, the increasing modes in these three environmental media are complicated.

Table 2. Ablation Depth of Sample Surface Processed in Different Media (μm)

N	**1**	**5**	**20**	**100**	**400**
Air	0.402 ± 0.001	3.058 ± 0.001	12.418 ± 0.001	38.061 ± 0.001	45.735 ± 0.001
Water	0.793 ± 0.001	1.107 ± 0.001	1.178 ± 0.001	8.542 ± 0.001	35.776 ± 0.001
Methanol	2.933 ± 0.001	4.571 ± 0.001	4.222 ± 0.001	5.271 ± 0.001	31.023 ± 0.001

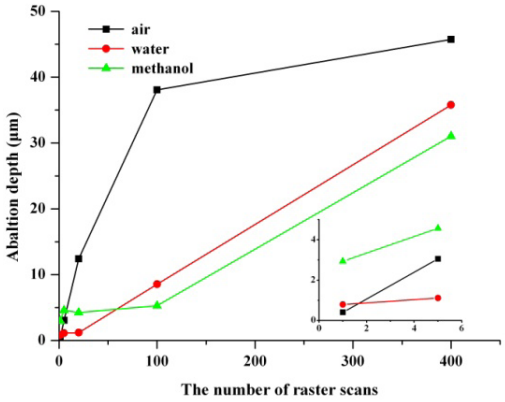

Fig. 5. Evolution of ablation depth versus number of raster scans in air, water, and methanol.

Before laser irradiation, the original surface states were the same in these three environmental media. Figure 6 shows a typical SEM image of sample surface before irradiation. Thus, the effect of surface roughness on ablation rate can be ignored when $N = 1$.

When $N = 1$, the ablation rate, defined as the ablation depth per laser pulse, was higher in methanol and water than in air. This observation is the same with that reported in other literature studies[28–30] which were performed in $N = 1$. One possible reason for higher ablation rate in liquid when $N = 1$ was that the effect of plasma confinement on the laser ablation was enhanced due to the presence of liquid. A previous study[31]reported that, compared with laser ablation in air, the plasma size and duration were much reduced when ablating in water. The plasma cannot interact with the first fs laser pulse because the plasma is generated after several nanoseconds. However, it can interact with the following pulses which have an interval of 1 ms with the previous pulse. The shorter duration of plasma can reduce the overlap between the plasma and the following laser pulses[32]. These factors weaken the plasma shielding effect, causing a stronger coupling of laser beam with the material. Thus, in the case of liquid environment the laser energy loss due to the plasma absorption was much reduced. More energy was hence being channeled deeper into the substrate. The material removal efficiency can therefore be enhanced in liquid.

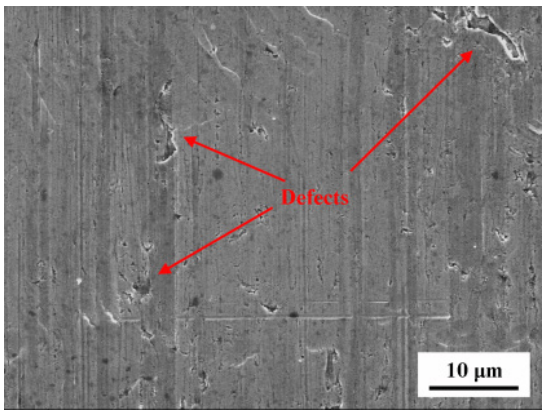

Fig. 6. Typical SEM image of sample surface before irradiation.

On the other hand, the plasma was confined in the liquid, resulting in higher acoustic and shock waves than the dry condition. In addition, bubble formation was observed in the liquid layer above the target during the ablation process due to the rapid temperature increase in liquid induced by the heat conduction of target material. Laser-induced shock wavesand the generation and collapse of vapor bubbles in the vicinity of the liquid–solid interface enhanced the impact pressure against the surface, and consequently, enhanced the ablation rate.

Furthermore, in liquid-mediated irradiations, the laser would be reflected at both air–liquids and liquids–solid interfaces. While in air, the reflection only occurs at air–solid interface. Liu *et al.*[29] evaluated the energy loss caused by the interfacial reflection and they found that for the same incident laser fluence, the reflection-induced energy loss in ambient air is higher than in liquid. It means that more energy can be injected into the sample surfaces due to the presence of liquids, resulting in the increase in ablation depth.

The water has a higher EVP than methanol which leads to more heat loss during laser ablation. Besides, methanol is more volatile than water and produces stronger shock wave impact pressure. These would account for the lower ablation rate when applying water than methanol when $N = 1$.

However, when $N = 5$, the ablation rate was higher in air than in water. This point proves that besides ablation medium, surface morphology is also a crucial factor that affects ablation rate. During multiple raster scans, surface roughness would be changed after each raster scan so that it will affect the absorption of subsequent laser pulses. After the first raster scan, the surface morphology has been changed significantly compared with original sample surface (Figs. 1(a) and (f)). Submicrometer ripples and much higher surface roughness have been induced by fs laser ablation. At the subsequent raster scans, these would affect the incident laser energy deposited on the irradiated surface. As shown in Figs. 1(a) and (f), the surface acquired in air was more rough and irregular than in water when $N = 1$. Generally, smooth metal surface has higher reflectivity of light than rough metal surface. In this situation, more laser energy was absorbed by the surface acquired in air than in water due to higher laser absorptance of laser caused by the trapping of laser and scattering. The increase inabsorbed laser energy caused by surface roughness in air was much higher than the increase in absorbed laser energy caused by liquid in water. Thus, the ablation rate was higher in air than in water when $N = 5$.

Nevertheless, this situation did not happen in methanol. On one hand, the surface structures acquired when $N = 1$ in methanol were also rough and irregular submicrometer ripples (Fig. 1(k)). On the other hand, when using methanol as ablation medium, the ablation rate

would increase due to the presence of liquid. Thus, in this situation, it was mainly because of the presence of liquid that the ablation rate was higher in methanol than in air.

For $20 \le N \le 100$, the ablation rate in air was much higher than that in liquid. As shown in Figs. 1–4, between $20 \le N \le 100$, the randomly distributed or linked *N*-mounds formed in air, while the surface processed in water was covered by ripples and that in methanol was covered by protruded ripples and grooves. Due to the presence of *N*-mounds, preferential ablation happened. Preferential ablation is an ablation process driven by surface geometric effect in which laser incident on the sidewalls of *N*-mounds is reflected into the valleys between *N*-mounds, resulting in increased laser fluence and a corresponding increase in ablation rate of the valleys[33]. Besides, laser that hits the sidewalls of the *N*-mounds has higher incident angle and reflectivity increases with incident angle. Subsequent laser pulses therefore preferentially removed materials between *N*-mounds, resulting in the deepening of the valleys. Once the linked *N*-mounds formed, they had focus effect on the incident laser, that is, when subsequent laser pulses irradiated the linked *N*-mounds, the incident laser was reflected into the valleys by the sidewalls of the *N*-mounds (Fig. 7). Moreover, based on the geometry of the linked *N*-mounds, light would experience multi-reflection by the linked *N*-mounds when irradiated the ablated sample surface, resulting in amplification of light absorptance of the structured sample surface. The linked *N*-mounds acted to focus the light into the valleys between them, significantly raising the laser fluence and then the ablation depth in the valleys. The ablation depth defined here is the perpendicular distance from the untreated sample surface to the lowest point of each ablated section. Thus, the deepening of the valley resulted in corresponding increase in the ablation depth of the entire irradiated area. With the increase in the aspect ratio of *N*-mounds, the focus effect will be enhanced.

On the contrary, the surfaces processed in liquids have no highly protruded structures. In this point, even though liquid can enhance ablation efficiency, because their laser strengthening effect caused by surface structures were much weaker, ablation rates in liquids were much less than that in air. However, in $N = 100$, the ablation rate was smaller in methanol than in water for the reason that methanol is volatile; under the irradiation of thousands of fs laser pulses, the loss of methanol was heavy. Thus, the effect of methanol on the enhancement of ablation efficiency decreased with the loss of methanol.

For $N = 400$, compared with $N = 100$, there were no significant differences in ablation rates in the three environmental media. An important factor that affected the ablation depth was the redeposition of ejected ablated materials. In liquid, the redeposited ablated materials were removed from the surface by the thermal convection currents and bubble-induced liquid motion. The bubble generation would also be accompanied with shock waves, which would provide additional force to clean off the debris induced by laser ablation. The amount of debris and redeposition of ablated materials in the surface was therefore reduced in liquid. However, the accumulation of ablated materials on the surface in air was serious without the assistance of liquid. Comparing Fig. 2(b) with Figs. 3(b) and 4(b), after $N = 100$, the surface structures in air present upward growth tendency which is caused by the redeposition of ablated materials. Ablated materials from the valleys redeposited onto the surface of the mounds and then they were sintered together by subsequent laser pulses and attached to the mounds, forming layers of nanostructures covering the mounds. With the increase in *N*, the thickness of sintered ablated material redeposited on the mounds increased due to accumulative effect, causing *N*-mounds to grow taller. This process also caused that the calculated ablation depth when $N = 400$ in air was not significantly different from that in liquids.

In conclusion, we investigate fs laser ablations of SS under single raster scan and multiple raster scans in air, water, and methanol media. Under single raster scan, the ablation rate is higher in liquid than in air due to the confinement of plasma, laser-induced shock-waves, and bubble-related mechanical forces. However, under multiple raster scans, the variation in ablation rate with the increasing number of raster scans in these three environmental media is complicated and is determined by the ablation medium as well as the surface morphology induced by previous fs laser raster scans. When $N > 20$, the ablation rate is much higher in air than in liquids due to preferential ablation caused by the formation of nanostructures-textured mound-shaped microstructures in air. Besides, the redeposition of ejected ablated materials is also an important factor that affects the ablation depth.

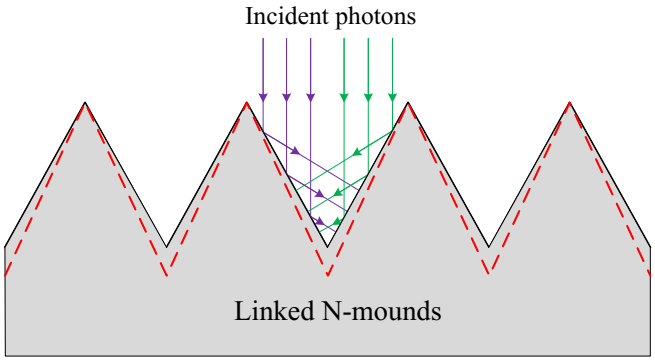

Fig. 7. Focus effect of linked *N*-mounds formed when $N > 20$ in air. The dashed lines show the possible outline of resulting linked *N*-mounds after irradiation.

This work was supported by the National Natural Science Foundation of China under Grant No. 51305292.

References

1. A. Y. Vorobyev and C. L. Guo, Laser Photon. Rev. **7,** 385 (2013).
2. A. Y. Vorobyev and C. L. Guo, Phys. Rev. B **72,** 195422 (2005).
3. S. Zhang, X. Hu, Y. Liao, F. He, C. Liu, and Y. Cheng, Chin. Opt. Lett. **11,** 033101 (2013).
4. B. Dusser, Z. Sagan, H. Soder, N. Faure, J.P. Colombier, M. Jourlin, and E. Audouard, Opt. Express **18,** 2913 (2010).
5. B. Wu, M. Zhou, and J. Li, Appl. Surf. Sci. **256,** 61 (2009).
6. F. Kong, Y. Jin, S. Liu, S. Chen, H. Guan, K. He, Y. Du, and H. He, Chin. Opt. Lett. **11,** 102302 (2013).
7. T. Y. Hwang, A. Y. Vorobyev, and C. L. Guo, Opt. Express A **19,** 824 (2011).
8. J. W. Yao, C. Y. Zhang, and H. Y. Liu, Appl. Surf. Sci. **258,** 7625 (2012).
9. T. L. Chang, Z. C. Chen, and Y. C. Lee, Opt. Express **20,** 15997 (2012).
10. E. V. Golosov, A. A. Ionin, Y. R. Kolobov, S. I. Kudryashov, A. E. Ligachev, Y. N. Noboselov, L. V. Seleznev, and D. V. Sinitsyn, J. Exp. Theor. Phys. **14,** 113 (2011).
11. M. S. Ahsan and M. S. Lee, Opt. Eng. **51,** 121815 (2012).
12. C. Albu, A. Dinescu, M. Filipescu, M. Ulmeanu, and M. Zamfirescu, Appl. Surf. Sci. **278,** 347 (2013).
13. L. S. Jiao, E. Y. K. Ng, and H. Y. Zheng, Appl. Surf. Sci. **264,** 52 (2013).
14. X. Jia, Y. Yuan, D. Yang, T. Jia, and Z. Sun, Chin. Opt. Lett. **12,** 113203 (2014).
15. M. S. Ahsan, Y. G. Kim, and M. S. Lee, J. Laser Micro/Nanoeng. **7,** 164 (2012).
16. S. Bashir, M. S. Rafique, C. S. Nathala, and W. Husinsky, Appl. Surf. Sci. **290,** 53 (2014).
17. A. Y. Vorobyevand C. L. Guo, Appl. Surf. Sci. **253,** 7272 (2007).
18. T. Y. Hwangand C. L. Guo, J. Appl. Phys. **111,** 083518 (2012).
19. B. K. Nayak, M. C. Gupta, and K. W. Kolasinsk, Nanotechnology **182,** 19530 (2007).
20. C. A. Zuhlke, T. P. Anderson, and D. R. Alexander, Appl. Surf. Sci. **283,** 648 (2013).
21. B. K. Nayakand M. C. Gupta, Opt. Laser. Eng. **48,** 966 (2010).
22. M. Momcilovic, J. Limpouch, V. Kmetik, and R. Redaelli, Appl. Surf. Sci. **258,** 8908 (2012).
23. C. Wang, H. B. Huo, M. Johnson, and M. Y. Shen, Nanotechnology **21,** 75304 (2010).
24. G. D. Miyaji, K. Z. Miyazaki, K. F. Zhang, and T. K. Yoshifuji, Opt. Express **20,** 14848 (2012).
25. M. Y. Shen, C. H. Crouch, J. E. Carey, and E. Mazur, Appl. Phys. Lett. **23,** 5694 (2004).
26. Y. Ju, C. Liu, Y. Liao, Y. Liu, L. Zhang, Y. Shen, D. Chen, and Y. Cheng, Chin. Opt. Lett. **11,** 072201 (2013).
27. L. Jiang and H. L. Tsai, in *Proceedings of NSF Workshop on Unsolved Problems and Research Needs in Thermal Aspects of Material Removal Processes* (2003).
28. M. E. Shasheen, J. E. Gagnon, and B. J. Fryer, J. Appl. Phys. **113,** 213106 (2013).
29. H. W. Liu, F. Chen, X. H. Wang, Q. Yang, H. Bian, J. H. Si, and X. Hou, Thin Solid Films **518,** 5188 (2010).
30. L. S. Jiao, E. Y. K. Ng, L. M. Wee, and H. Y. Zheng, Appl. Phys. A **104,** 1081 (2011).
31. G. Y. Mak, E. Y. Lam, and H. W. Choi, Appl. Phys. A **102,** 441 (2011).
32. L. S. Jiao, E. Y. K. Ng, L. M. Wee, and H. Y. Zheng, Phys. Proc. **19,** 426 (2011).
33. C. A. Zuhlke, T. P. Anderson, and D. R. Alexander, Opt. Express **21,** 8460 (2013).